

## Evaluation of a mixed columnar-equiaxed solidification model with laboratory castings

This article has been downloaded from IOPscience. Please scroll down to see the full text article.

2012 IOP Conf. Ser.: Mater. Sci. Eng. 27 012018

(<http://iopscience.iop.org/1757-899X/27/1/012018>)

View [the table of contents for this issue](#), or go to the [journal homepage](#) for more

Download details:

IP Address: 178.191.204.136

The article was downloaded on 31/05/2013 at 10:06

Please note that [terms and conditions apply](#).

## Evaluation of a mixed columnar-equiaxed solidification model with laboratory castings

M Wu<sup>1,2</sup>, G Nunner<sup>1</sup>, A Ludwig<sup>1</sup>, J Li<sup>3</sup> and P Schumacher<sup>c</sup>

<sup>1</sup>Chair of Simulation & Modelling of Metallurgical Processes,

<sup>2</sup>Christian-Doppler Lab for Adv. Process Simulation of Solidification & Melting,

<sup>3</sup>Chair of Casting Research,

University of Leoben, Franz-Josef-Str. 18, A-8700 Leoben, Austria

E-mail: menghuai.wu@unileoben.ac.at

**Abstract.** This work evaluates a mixed columnar-equiaxed solidification model [Wu et al. 2010 *Comp. Mater. Sci.* **50** 32] by comparison with the laboratory castings. In the numerical model nucleation of equiaxed crystals, tracking of the position of columnar primary dendrite tips, transition from non-dendritic to dendritic growth, columnar-to-equiaxed transition (CET), melt flow and grain sedimentation are taken into account. As modeling result the as-cast structure, macrosegregation, volume-averaged inter- and extra-dendritic eutectic phase can be calculated. In the laboratory experiment a series of Al-Cu ingots with different pouring parameters and compositions were cast, and the corresponding structural information and macrosegregation were analyzed. The primary goals are (1) to explore the uncertainties and limitation of the numerical model; (2) to identify the sensitive parameters influencing the casting and modeling results; finally (3) to further justify the model assumptions.

### 1. Introduction

Typical as-cast structure of engineering castings includes the chill zone, columnar zone and center equiaxed zone. Empirical knowledge about the formation of the as-cast structure, mostly obtained before 1980s [1-5], rests primarily on two critical issues: one is the origin of the equiaxed crystals; the other is the columnar-to-equiaxed transition (CET). The most-likely-operating nucleation mechanisms were proposed: (1) the heterogeneous nucleation [6]; (2) the 'big band' theory [1]; (3) the partial remelting of columnar dendrites [7]; (4) the showering down of dendrite crystals formed from the casting top surface [8]; (5) the so-called 'separation' theory [3] which has some similarity to the 'big band' theory. Progress was also made in the understanding of CET since the pioneering work of Hunt [9] in 1980s. A CET map, the correlation of the columnar primary dendrite tip growth velocity with the local temperature gradient at the moment of CET, was established to predict the occurrence of CET. This CET map was later confirmed and further improved by many authors [10-15]. In the meantime people also tried to abstract some empirical correlations as indirect criteria to predict the CET for engineering castings [16-20].

Unfortunately, the application of the theories above or empirical knowledge was very limited, as the flow and crystal transport were not considered. Therefore, a 5-phase mixed columnar-equiaxed solidification model was recently proposed by the current authors [21-25] on the base of modeling the multiphase transport phenomena. Promisingly, the typical grain structure of the Al-Cu cylindrical

ingots, often observed experimentally [1, 3, 5], was preliminarily simulated [21-22, 25]. The motivation of the current work is to evaluate the mixed columnar-equiaxed solidification model by comparison with laboratory castings. Therefore, some classical experiments on the Al-Cu ingot casting were repeated and the as-cast structural information including distinct columnar and equiaxed zones, macrosegregation, and grain size distribution was analyzed.

## 2. Key features of the numerical model

As depicted in figure 1, two types of crystal morphologies co-exist: equiaxed and columnar. We assume that immediately following the nucleation of crystals in the chill zone, columnar dendrites start to grow from the casting surface. Three ‘hydrodynamic’ phases, denoted as e-, c- and  $\ell$ -phases, are considered and quantified with their volume fractions,  $f_e$ ,  $f_c$ ,  $f_\ell$ . They move with corresponding velocities,  $\bar{u}_e$ ,  $\bar{u}_c$ , and  $\bar{u}_\ell$ . Here  $\bar{u}_c$  is predefined (zero in the case of ingot casting), while  $\bar{u}_e$  and  $\bar{u}_\ell$  are solved numerically.

A three-parameter heterogeneous nucleation law [26] is applied for the origin of equiaxed grains. With a free-slip boundary condition for the e-phase, the equiaxed grains attached on casting surfaces (top or side wall) are allowed to be swept away by the melt flow into the bulk region. Almost all the aforementioned nucleation mechanisms [1, 3, 6, 8] can be taken into account except for the one due to partial remelting of columnar dendrites [7]. As the current model does not include mold filling, hence a simple idea is proposed to consider the equiaxed nuclei which have formed during mold filling, i.e. to pre-set an initial grain number density in the as-filled state,  $n_0$ .

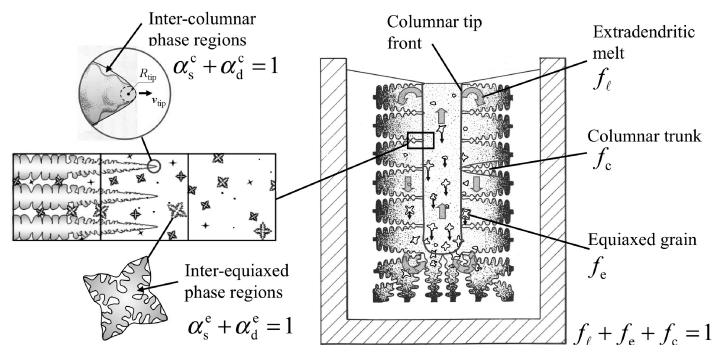


**Figure 1.** Schematic of the mixed columnar-equiaxed solidification in an ingot casting

Dendritic crystal growth is considered. Two distinct phase regions exist within the envelope of an equiaxed grain or a columnar trunk: the solid dendrites and interdendritic melt. It is assumed that the interdendritic melt is transported with the solid dendrites and is generally more enriched with solute elements than the extradendritic melt surrounding the crystals. In this sense, a fictitious crystal boundary envelope is constructed to separate the interdendritic melt from the extradendritic melt. Therefore, five ‘thermodynamic’ phase regions are defined in the system: the solid dendrites and interdendritic melt in the equiaxed grain, the solid dendrites and interdendritic melt in the columnar dendrite trunk, and the extradendritic melt. They are quantified with their volume fractions,  $f_s^c$ ,  $f_d^c$ ,  $f_s^e$ ,  $f_d^e$ ,  $f_\ell$ , and characterized by their corresponding solute concentrations,  $c_s^e$ ,  $c_d^e$ ,  $c_s^c$ ,  $c_d^c$ ,  $c_\ell$ . Inside an equiaxed grain, volume fractions of interdendritic liquid and solid dendrites are quantified respectively with  $\alpha_d^e$ ,  $\alpha_s^e$ , hence  $f_d^e = \alpha_d^e \cdot f_e$  and  $f_s^e = \alpha_s^e \cdot f_e$ . Inside a columnar dendrite trunk,  $f_d^c = \alpha_d^c \cdot f_c$  and  $f_s^c = \alpha_s^c \cdot f_c$ .

Both hard blocking [9] and soft blocking [12] mechanisms are implemented to model the columnar-to-equiaxed transition (CET). The hard blocking mechanism suggests that CET might occur when the equiaxed grains ahead of the columnar dendrite tip exceeds a critical volume fraction ( $f_{e,CET} = 0.49$ ). A recent study [27] has shown that the critical value suggested by Hunt [9] might be too large. Instead, a value of  $f_{e,CET} = 0.2$  should be used. The soft blocking mechanism suggests that the exhausting of the growth driving force (constitutional undercooling) due to the enrichment of solute elements (rejected by the growing equiaxed grains) stops the growth of columnar primary dendrite tips. Details regarding to the growth kinetics, treatment of the dendritic morphology of crystals, algorithm of tracking the columnar tip, etc. refer to previous publications [21-22].

### 3. Casting and simulation parameters

Casting configuration is shown in figure 2. A specially manufactured (non-grain-refined and unmodified) Al-Cu alloy is prepared from commercially pure aluminum and copper (99.99 wt.%). The alloy is limited to a binary system with proper compositions (2.0 wt.%Cu, 4.0 wt.%Cu). A clay bonded graphite crucible is used as casting mold. Casting conditions are listed in table 1. After solidification the ingot is subjected to following analyses: (1) macrostructure; (2) macrosegregation; (3) microstructure (grain size and phase fraction). Thermo-physical and dynamic properties used for the calculations refer to [21-22]; some process parameters are summarized in table 2.

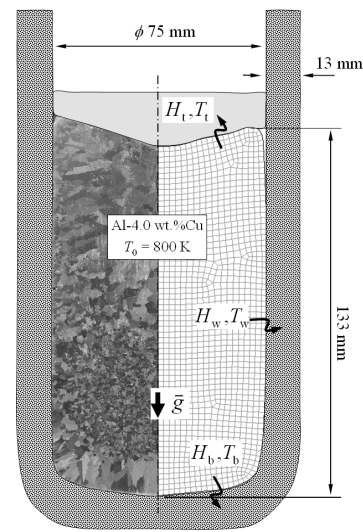


**Figure 2.** Configuration of the casting geometry and boundary conditions.

**Table 1.** Sample ingots characterized by nominal copper content

| Ingot number       | 1#  | 2#  | 3#  | 4#  | 5#  | 6#  | 7#  | 8#  |
|--------------------|-----|-----|-----|-----|-----|-----|-----|-----|
| Alloys (wt.%Cu)    | 2.0 | 2.0 | 2.0 | 2.0 | 4.0 | 4.0 | 4.0 | 4.0 |
| Touring temp. (°C) | 700 | 750 | 800 | 810 | 700 | 750 | 800 | 808 |
| Mold temp. (°C)    | 20  | 20  | 20  | 20  | 20  | 20  | 20  | 20  |

**Table 2.** Process parameters used for the simulations.

| Initial and boundary conditions:                          |                       | Nucleation parameters:                              |  |
|---|-----------------------|---|--|
| $c_0 = 2.0$ and $4.0$ wt.%                                | $T_0$ see Table 1     | $n_{max} = 10^{11} \text{ m}^{-3}$                  | $\Delta T_N = 3.5 \text{ K}$                 |
| $H_t = 10 \text{ W}\cdot\text{m}^{-2}\cdot\text{K}^{-1}$  | $T_t = 290 \text{ K}$ | $\Delta T_\sigma = 0.5 \text{ K}$                   | $n_0 = 10^7, 10^8$ and $10^9 \text{ m}^{-3}$ |
| $H_w = 200 \text{ W}\cdot\text{m}^{-2}\cdot\text{K}^{-1}$ | $T_w = 290 \text{ K}$ | Morphological shape factors & dendrite arm spacing: |  |
| $H_b = 300 \text{ W}\cdot\text{m}^{-2}\cdot\text{K}^{-1}$ | $T_b = 290 \text{ K}$ | $\Phi_{env}^c = 0.48$                               | $\Phi_{enh}^c = 0.4$                         |
|   |                       | $\Phi_{env}^c = 0.80$                               | $\Phi_{circ}^c = 0.5$                        |
|   |                       |   | $\lambda_1 = 500 \mu\text{m}$                |
|   |                       |   | $\lambda_2 = 100 \mu\text{m}$                |

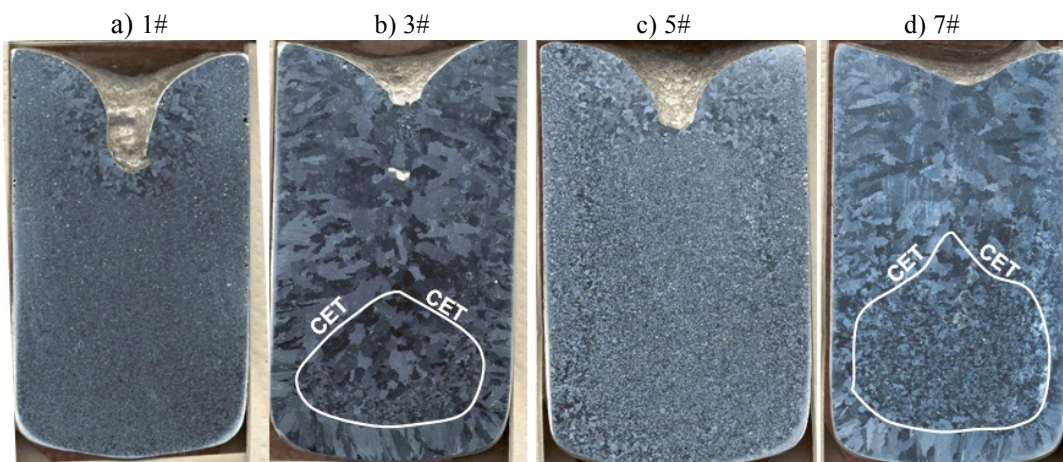


**Figure 3.** Examples of as-cast macrostructure of the Al-Cu ingots

#### 4. Results and discussions

Characteristic macrostructures of the sample ingots 1#, 3#, 5# and 7# (table 1) and their corresponding simulation results are shown in figures 3 and 4. For the ingots poured at high temperature ( $T_0 = 800$  °C), both as-cast structures (figure 3, #3 and #7) and simulation results (figure 4, #3 and #7) have shown that there is a well-developed columnar zone in the upper part and near the casting surface region of the ingot. In the lower bottom region a pure equiaxed zone separated from columnar zone by the CET line can be found. The macrostructure distribution patterns of both experimental and simulation results agree with each other. Quantitatively, the numerically predicted equiaxed zone is smaller than the experimental ones.

For the ingots poured at low temperature ( $T_0 = 700$  °C), the simulation results (figure 4, #1 and #5) do not agree with the as-cast structure (figure 3, #1 and #5). The as-cast structure is found to be almost fully equiaxed, while the simulation shows a mixed columnar-equiaxed structure. Both numerical simulation and experimental results have confirmed that the lower pouring temperature is favour of the formation of equiaxed zone, but the numerically predicted equiaxed zone in the ingot poured at 700 °C is far too small in comparison to the experimentally observed equiaxed zone.

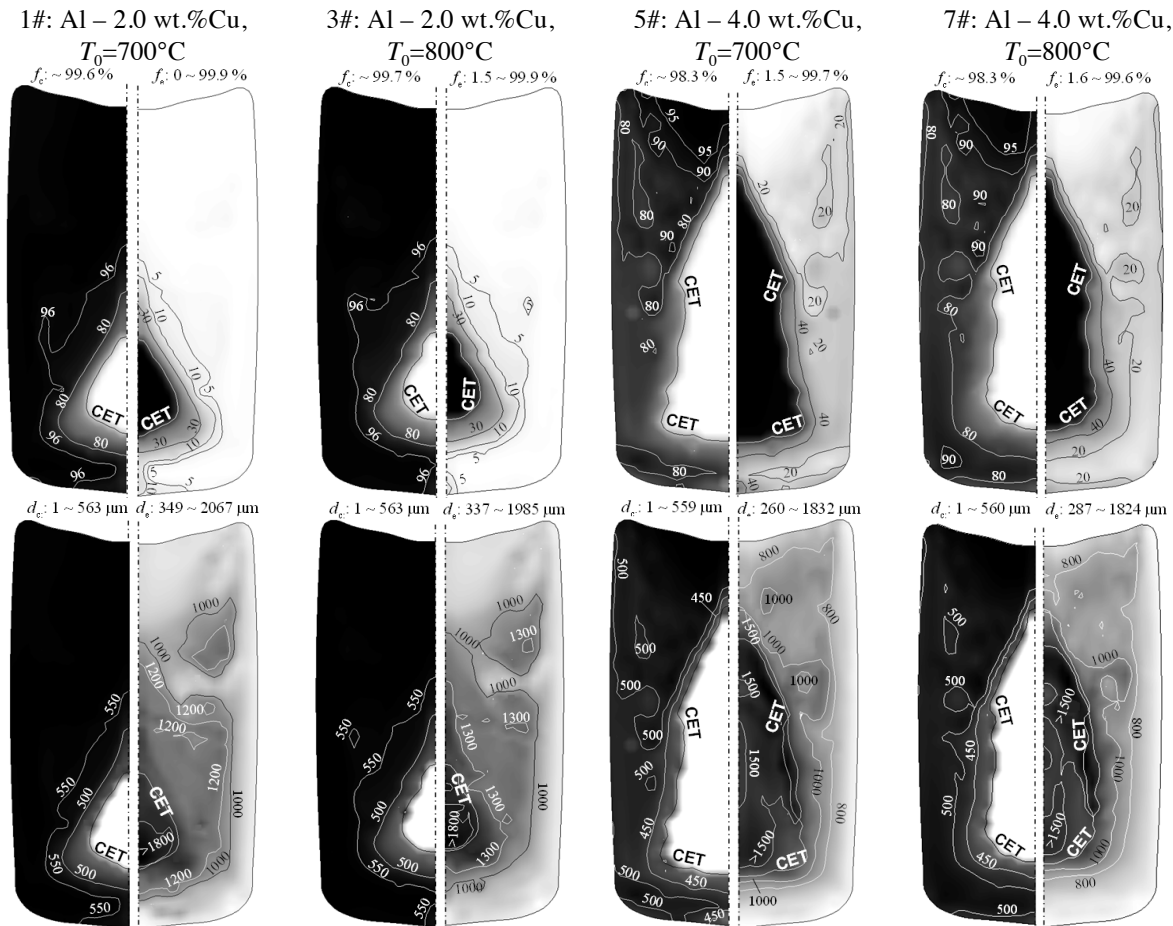


**Figure 4.** Calculated macrostructure of the ingots, corresponding to 1#, 3#, 5# and 7# in figure 3. Four quantities are present: the volume fraction of columnar phase  $f_c$  [vol.%], equiaxed phase  $f_e$  [vol.%], diameter of columnar trunk  $d_c$  [ $\mu\text{m}$ ], and equiaxed grain size  $d_e$  [ $\mu\text{m}$ ]. All quantities are shown in gray scale (dark for the highest and light for the lowest value). The position of CET is also marked. All simulations were performed with the same equiaxed grain nucleation parameters (Table 2), and  $n_0 = 10^7 \text{ m}^{-1}$ . The hard blocking criterion for CET is  $f_{e,\text{CET}} = 0.49$ .

Further numerical parameter studies were performed to investigate the discrepancy between the numerical model and experiment. Above simulations were made with an assumption of the same and constant nucleation parameters ( $n_{\max}$ ,  $\Delta T_N$ ,  $\Delta T_\sigma$ ,  $n_0$ ) despite of the difference in pouring temperature. This assumption might not be valid. The initial number density of equiaxed grains  $n_0$  is mainly originated from the nucleation during pouring. The current model has considered the equiaxed nuclei, which have formed during mold filling by pre-setting an initial  $n_0$ . According to ‘big band’ [1] or ‘separation’ theory [3], large amount of equiaxed nuclei would be produced during pouring when the melt comes in first contact with the cold mold. Those nuclei would be further brought and dispersed in the bulk melt. The lower the pouring temperature, the more nuclei would be created initially with this mechanism. In order to verify this hypothesis, simulations by varying  $n_0$  (from  $10^{+7}$  to  $10^{+9}$ ) for the lower casting temperature ( $T_0 = 700$  °C) were made. As expected (see figure 5), the pure equiaxed zone, enclosed in the CET line, increases significantly with the increase of  $n_0$ . The current paper cannot verify the value of  $n_0$ , but this study indicates the importance of the pouring process (method and temperature) in the macrostructure formation. Based on the above modeling results, the experimentally observed phenomenon about the influence of the pouring temperature on the size of the equiaxed crystal zone in the casting center might be explained as follows: firstly, the low pouring temperature is in favor of the heterogeneous nucleation of the equiaxed crystals; secondly, the initial number of the crystals created during pouring at a lower pouring temperature is larger than the number of crystals created at a higher pouring temperature.

Figure 6 shows the influence of the CET hard blocking criterion on the macrostructure. Obviously, the predicted pure equiaxed zone by using  $f_{e,CET}=0.2$  is much more close to the experiment (figure 3c). This result seems to confirm the finding of Martorano et al. [27] that CET hard blocking criterion ( $f_{e,CET}$ ) should better be 0.2 rather than 0.49.

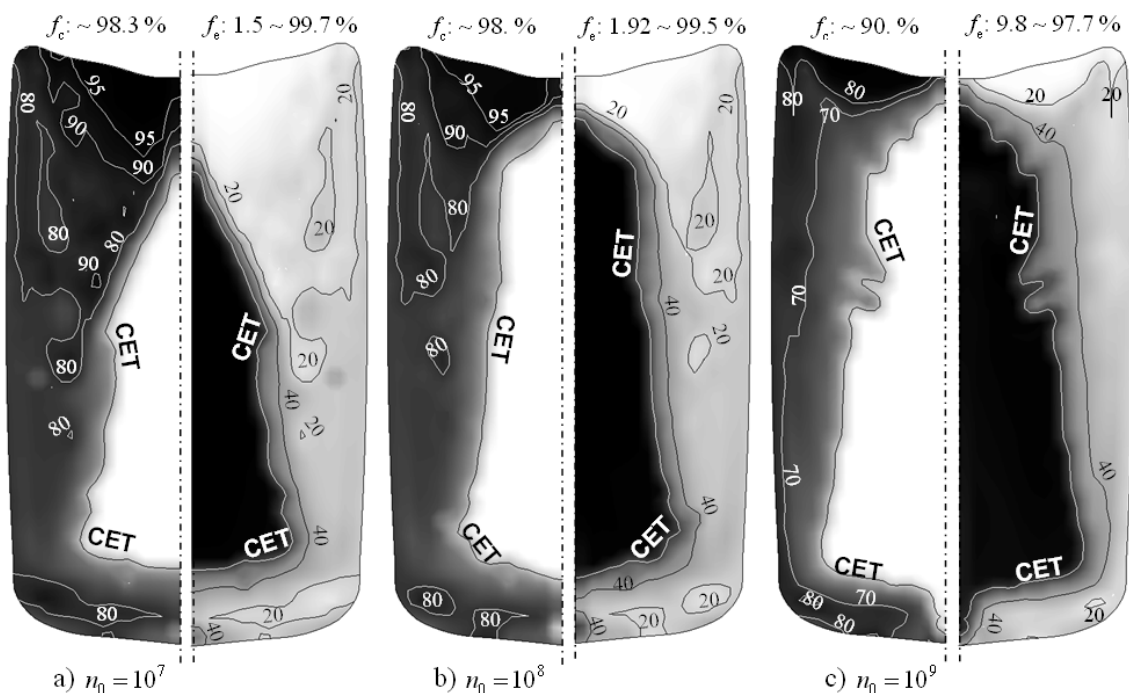


**Figure 5.** Influence of  $n_0$  on the macrostructure: a)  $n_0 = 10^{+7}$ , b)  $n_0 = 10^{+8}$ ,  $n_0 = 10^{+9}$ . Ingot #5, Al-4.0 wt.%Cu, poured at 700 °C. Two quantities are present: left for  $f_c$  [vol.%], right for  $f_e$  [vol.%]. All quantities are shown in gray scale (dark for the highest and light for the lowest value). CET position is plotted as well.

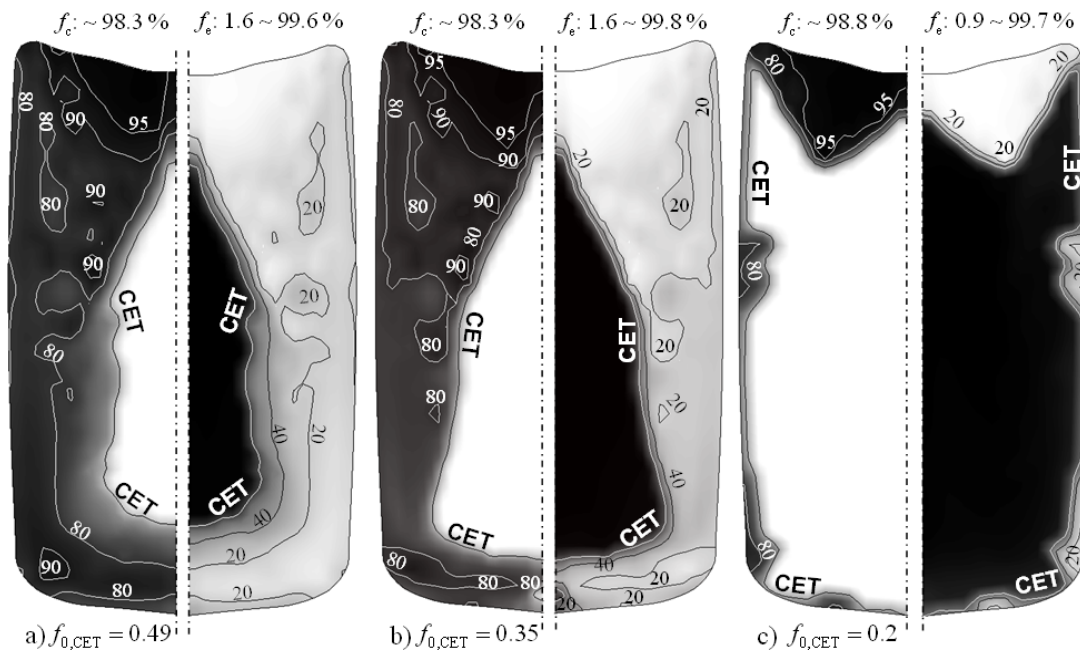


**Figure 6.** Influence of the CET hard blocking criterion on the macrostructure: a)  $f_{e,CET} = 0.49$ , b)  $f_{e,CET} = 0.35$ , c)  $f_{e,CET} = 0.2$ . Ingot #5, Al-4.0 wt.%Cu, poured at 700 °C. Two quantities are present: left for  $f_c$  [vol.%], right for  $f_e$  [vol.%]. All quantities are shown in gray scale (dark for the highest and light for the lowest value). CET position is plotted as well.

The measured and predicted macrosegregation patterns for the sample #7 (see figure 7) have shown some similarities and discrepancy. The similarities are: relatively lower  $c_{mix}$ , i.e. negative segregation, in the equiaxed zone enclosed by the CET line, some discontinuous islands of higher  $c_{mix}$ , i.e. positive segregation, in the upper part of the ingot. The main discrepancy between the model and the experiment is the severity of the macrosegregation: the measured  $c_{mix}$  varies from 3.67 to 4.31, while the calculated  $c_{mix}$  varies from 3.92 to 4.05. The main reasons for this discrepancy might come from the inaccurate prediction of the flow and sedimentation, and the assumed crystal morphological shape factors, which plays important role in the calculation of the species exchange between the inter- and extradendritic melts. Study and discussion of this topic cannot be covered by the current paper.

## 5. Summary

The macrostructure of Al-Cu ingot was verified to be reproducible by the newly developed mixed columnar-equiaxed solidification model, although the detailed structural quantities did not yet match the experiment quantitatively. Previous knowledge [1-8] has confirmed the importance of the nucleation events, which seems to be strongly influenced by the process variables like pouring method and pouring temperature. Modeling results have shown that the most sensitive parameters

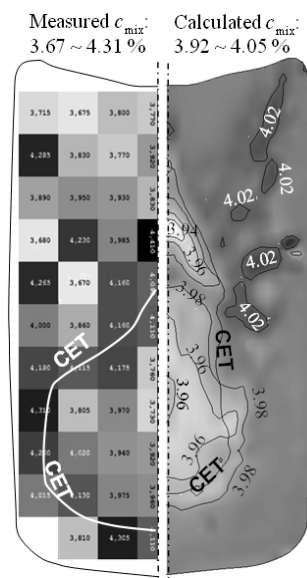


**Figure 7.** Comparison of the measured (spark analysis) macrosegregation with the calculated one. Ingot #7, Al-4.0 wt.%Cu, poured at 800 °C.  $c_{mix}$  is shown in gray scale (dark for the highest and light for the lowest value). CET positions are plotted.

for the macrostructure are the nucleation parameters such as the initial number of the crystals created during pouring,  $n_0$ , the maximum potential nucleation sites,  $n_{\max}$ , etc. Effect of grain refiner and inoculation is not studied here. In the modeling point of view another sensitive factor for the macrostructure is the hard blocking criterion  $f_{e,CET}$ , for which a value smaller than the originally suggested 0.49 [9] should rather be used, e.g. 0.2 [27]. The current work is still going on, and further evaluations and more detailed analyses of the modeling and experimental results will be presented later.

## References

- [1] Chalmers B 1963, *J. Austral. Inst. Met.* **8** 255
- [2] Flemings M 1974 *Solidification Processing* (New York: McGraw-Hill)
- [3] Ohno A 1987 *Solidification: The Separation Theory and its Practical Applications* (Berlin: Springer-Verlag)
- [4] Spittle J, Dellamore G and Smith R 1967 *Proc. The Solidification of Metals (The Iron and Steel Institute London)* 318
- [5] Morando R, Biloni H, Cole G and Bolling G 1970 *Metall. Trans.* **1** 1407
- [6] Winegard W and Chalmers B 1954 *Trans. ASM-AIME* **46** 1214
- [7] Jackson K, Hunt J, Uhlmann D, Seward III T 1966 *Trans. TMS-AIME* **236** 149
- [8] Southin R 1967 *Trans. TMS-AIME* **239** 220
- [9] Hunt J 1984 *Mater. Sci. Eng.* **65** 75
- [10] Gäumann M, Trivedi R and Kurz W 1997 *Mater. Sci. Eng. A* **226-228** 763
- [11] Wang C and Beckermann C 1994 *Metall. Mater. Trans. A* **25A** 1081
- [12] Martorano M, Beckermann C and Gandin Ch-A 2003 *Metall. Mater. Trans. A* **34A** 1657
- [13] Martorano M and Biscuola V 2009 *Acta Mater.* **57** 607
- [14] Wu M and Ludwig A 2006 *Metall. Mater. Trans. A* **37A** 1613
- [15] Wu M and Ludwig A 2007 *Metall. Mater. Trans. A* **38A** 1465
- [16] Gandin Ch-A. 2000 *Acta Mater.* **48** 2483
- [17] Gandin Ch-A 2000 *ISIJ Int.* **40** 971
- [18] McFadden A, Browne D and Gandin Ch-A 2009 *Metall. Mater. Trans. A* **40A** 662
- [19] McFadden A and Browne D 2009 *Applied Math. Modell.* **33** 1397
- [20] Siqueira C, Cheung N and Garcia A 2002 *Metall. Mater. Trans. A* **33A** 2107
- [21] Wu M, Fjeld A and Ludwig A 2010 *Comp. Mater. Sci.* **50** 32
- [22] Wu M, Ludwig A and Fjeld A 2010 *Comp. Mater. Sci.* **50** 43
- [23] Wu M and Ludwig A 2009 *Acta Mater.* **57** 5621
- [24] Wu M and Ludwig A 2009 *Acta Mater.* **57** 5632
- [25] Wu M and Ludwig A 2009 *Int. J. Cast Metals Research* **22** 323
- [26] Rappaz M 1989 *Int. Mater. Rev.* **34** 93
- [27] Martorano M and Biscuola V 2008 *Metall. Mater. Trans. A* **39A** 2885